Dauer pheromone and G-protein signaling modulate the coordination of intraflagellar transport kinesin motor proteins in *C. elegans*

Jan Burghoorn[1,*,‡], Martijn P. J. Dekkers[1,*,§], Suzanne Rademakers[1], Ton de Jong[2], Rob Willemsen[3], Peter Swoboda[4] and Gert Jansen[1,¶]

[1]Department of Cell Biology and Genetics, [2]Department of Pathology, [3]Department of Clinical Genetics, Erasmus MC, PO Box 2040, 3000 CA Rotterdam, the Netherlands
[4]Karolinska Institute, Center for Biosciences at NOVUM, Department of Biosciences and Nutrition, Hälsovägen 7, S-14157 Huddinge, Sweden
[‡]Present address: Karolinska Institute,Center for Biosciences at NOVUM, Department of Biosciences and Nutrition, Hälsovägen 7, S14157 Huddinge, Sweden
[*]These authors contributed equally to this work
[§]Present address: Biozentrum, University of Basel, Klingelbergstrasse 50/70, CH-4056 Basel, Switzerland
[¶]Author for correspondence (g.jansen@erasmusmc.nl)

Accepted 25 March 2010
Journal of Cell Science 123, 2077-2084

doi:10.1242/jcs.062885

Summary

Cilia length and function are dynamically regulated by modulation of intraflagellar transport (IFT). The cilia of *C. elegans* amphid channel neurons provide an excellent model to study this process, since they use two different kinesins for anterograde transport: kinesin-II and OSM-3 kinesin together in the cilia middle segments, but only OSM-3 in the distal segments. To address whether sensory signaling modulates the coordination of the kinesins, we studied IFT protein motility in *gpa-3* mutant animals, since dominant active mutation of this sensory Gα protein GPA-3QL) affects cilia length. In addition, we examined animals exposed to dauer pheromone, since dauer formation, which involves *gpa-3*, induces changes in cilia morphology. Live imaging of fluorescently tagged IFT proteins showed that in *gpa-3* mutants and in larvae exposed to dauer pheromone, kinesin-II speed is decreased and OSM-3 speed is increased, whereas structural IFT proteins move at an intermediate speed. These results indicate that mutation of *gpa-3* and exposure to dauer pheromone partially uncouple the two kinesins. We propose a model in which GPA-3-regulated docking of kinesin-II and/or OSM-3 determines entry of IFT particles into the cilia subdomains, allowing structural and functional plasticity of cilia in response to environmental cues.

Key words: IFT, Kinesin-II, OSM-3, *C. elegans*, G-protein signaling, Dauer pheromone

Introduction

Cilia are cellular protrusions that are present on almost all post-mitotic vertebrate cells. Cilia have important motility or sensory functions and are required for the organization of several signal transduction pathways. Structurally, cilia are dynamic. Ciliogenesis, cilium length and morphology and the organization of signaling pathways in cilia are regulated (Mukhopadhyay et al., 2008; Quarmby, 2004; Sorokin, 1962; Wang et al., 2006). Although genetic analyses have identified several kinases that modulate cilia length (Bengs et al., 2005; Berman et al., 2003; Burghoorn et al., 2007; Tam et al., 2007), little is known about the molecular mechanisms involved; however, intraflagellar transport (IFT) is a probable process (Blaineau et al., 2007; Dentler, 2005; Engel et al., 2009; Evans et al., 2006; Marshall et al., 2005; Pan and Snell, 2005). IFT is responsible for bi-directional transport of structural and signaling components of the cilia along a microtubular axoneme. Kinesin-II motors mediate anterograde transport from the transition zone, where the axoneme is anchored in the cell, to the tip of the cilium. Cytoplasmic dynein 1B moves the particles back. IFT particles consist of at least 18 proteins, arranged in two complexes, A and B.

The amphid channel cilia of *C. elegans* can be divided into a middle segment with nine doublet microtubules and a distal segment with nine singlet microtubules (Perkins et al., 1986). Two kinesin complexes, heterotrimeric kinesin-II and homodimeric OSM-3 kinesin (KIF17 in human), which both belong to the kinesin-2 family, mediate transport in the middle segments, whereas only OSM-3 mediates transport in the distal segments (Snow et al., 2004). This bipartite cilium structure in *C. elegans* could provide a mechanism for plasticity of sensory signaling during environmental or developmental changes, for instance by regulating the length of the cilia, or the localization of signaling molecules in the two segments.

Many environmental cues are detected by G-protein-coupled receptors (GPCRs) and relayed by heterotrimeric G proteins to intracellular responses. *C. elegans* has 21 Gα, two Gβ and two Gγ subunits (Cuppen et al., 2003; Jansen et al., 1999). To test whether these G-protein subunits play a role in cilia development, *C. elegans* with mutant genes for all these proteins have been tested for the uptake of fluorescent dyes in the amphid neurons (dye filling), a process that requires the presence of the sensory cilia (Jansen et al., 1999; Perkins et al., 1986; Zwaal et al., 1997). Only *gpa-3QL* animals, which carry a dominant active mutant form of the sensory Gα subunit gene *gpa-3*, showed a dye filling defective phenotype, suggesting that it might affect cilia development or maintenance (Zwaal et al., 1997). *gpa-3* is expressed in ten pairs of amphid sensory neurons, in the PHA and PHB phasmid neurons and in the AIZ and PVT interneurons, and plays a role in various sensory processes. GPA-3 also plays a role in dauer development, a developmental switch that allows *C. elegans* to survive under

harsh environmental conditions or overcrowding (Riddle and Albert, 1997). When exposed to dauer pheromone, a constitutively produced pheromone that probably serves as a measure of population density, *gpa-3(lf)* animals form fewer dauers than wild-type animals, while *gpa-3QL* animals constitutively form dauers (Zwaal et al., 1997). Interestingly, dauer development requires cilia and is accompanied by alterations in the position and structure of several cilia (Albert and Riddle, 1983).

In this study, we examined whether dauer pheromone and GPA-3 regulate IFT. Electron microscopy and fluorescence microscopy of GFP-labeled cilia revealed that the cilia of *gpa-3QL* animals are shorter, but cilia length in *gpa-3(lf)* animals was only slightly affected. Live imaging of IFT proteins fused with GFP showed uncoupling of the two kinesins in *gpa-3QL* and *gpa-3(lf)* animals and in larvae exposed to dauer pheromone. However, structural IFT particle proteins moved at speeds intermediate to the two kinesins. Our results show that an environmental cue, probably mediated by GPA-3, modulates the coordination of the two IFT kinesins. We propose that this mechanism allows the regulation of cilia length or the localization of proteins in specific ciliary subdomains.

Results

gpa-3QL affects cilia morphology

Zwaal et al. (Zwaal et al., 1997) have shown that animals that carry a dominant active mutation of *gpa-3*, *gpa-3QL(syIs24)* and *syIs25*, are dye-filling defective. To study the cilia morphology of *gpa-3QL* animals, we examined cross sections of the amphid channel cilia of wild-type, *gpa-3(lf)* and *gpa-3QL* animals, using electron microscopy (EM; Fig. 1). The cilia of wild-type animals looked as previously described (Fig. 1B-D) (Perkins et al., 1986; Ward et al., 1975) and we observed no defects in the cilia of *gpa-3(lf)* animals (results not shown). *gpa-3QL* animals exhibited a variety of morphological defects in the cilia (Fig. 1E-G; supplementary material Fig. S1). In the distal segments we could distinguish four or five cilia (instead of ten in wild-type animals). These distal segments contained much electron-dense material and some had smaller diameters. Only few microtubules could be discerned, perhaps because of the presence of the electron-dense material (Fig. 1E; supplementary material Fig. S1). Further proximally, at the beginning of the middle segments, more cilia could be seen (five to nine), some of which had smaller diameters and contained only few microtubules (Fig. 1F; supplementary material Fig. S1). Closer to the transition zone ten cilia could be distinguished, some of which had smaller diameters (Fig. 1G; supplementary material Fig. S1). Similar defects were observed in the amphid channel cilia of four *gpa-3QL* animals (supplementary material Fig. S1). In one of these animals the socket cell surrounding the cilia distal segments seemed more electron dense. The significance of this observation is not clear.

The EM analysis suggests that the amphid channel cilia of *gpa-3QL* animals are shorter and/or posteriorly displaced, although not all cilia are affected. To determine which cilia were affected, GFP was expressed in several amphid sensory neurons, using promoters that drive expression in a single or a restricted set of cells. Four constructs were transcriptional fusions: $p_{gpa\text{-}4}$*::gfp* [drives GFP expression in the ASI neurons (Jansen et al., 1999)], $p_{flp\text{-}6}$*::gfp* [in ASE (Li et al., 1999)], $p_{ops\text{-}1}$*::gfp* [in ASG (Sagasti et al., 1999)] and $p_{srh\text{-}142}$*::gfp* [in ADF (Sarafi-Reinach and Sengupta, 2000)]. In these cases GFP enters the cilia and probably localizes to the lumen. In addition, the cilia of the ASI neurons and of ASH, ASK and ADL were visualized using translational fusions, $p_{gpa\text{-}4}$*::gpa-4::gfp* and $p_{gpa\text{-}15}$*::gpa-15::gfp*, respectively, in which GFP is fused in frame to the first 46 or 40 N-terminal amino acids of the heterotrimeric Gα proteins GPA-4 or GPA-15 (Jansen et al., 1999). Since the N-terminal amino acids of Gα proteins are required for their localization at the membrane, we expect these GFP fusions to localize at the ciliary membrane. Finally, we used a $p_{gpa\text{-}4}$*::tbb-4::mCherry* construct to visualize the axoneme of the ASI cilia using a translational fusion between full length *tbb-4* and *mCherry*. *tbb-4* encodes a β-tubulin, which is part of the middle and distal segments of sensory cilia of *C. elegans*, but not the transition zone (Bae et al., 2006).

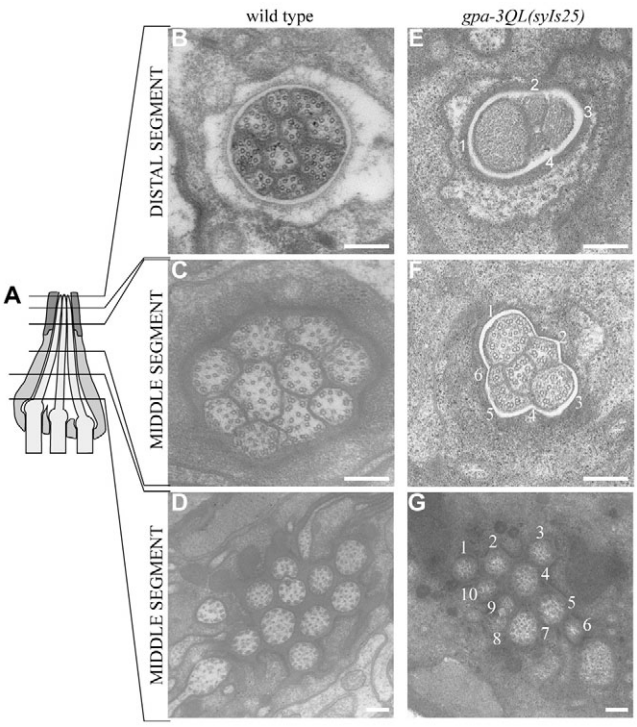

Fig. 1. *gpa-3QL* affects cilium length and morphology. (**A**) Schematic representation of three of the amphid channel cilia embedded in the sheath and socket cells. The approximate positions of the EM cross sections are indicated. (**B-D**) EM cross sections through the tip of an adult wild-type animal. (B) Section through the socket cell, showing the distal segments of the ten-channel cilia, which contain singlet microtubules. (C) Ten-channel cilia embedded in the sheath cell. (D) More posterior section through the middle segments reveals ten-channel cilia containing doublet microtubules. (**E-G**) EM cross sections through the tip of an adult *gpa-3QL(syIs25)* animal. In the distal segments of this *gpa-3QL* animal, only four cilia could be identified, containing much electron-dense material. (F) Section of a *gpa-3QL* animal through the socket cell, showing six cilia. Some cilia have a smaller diameter and contain singlet microtubules (e.g. cilium 6). (G) More posterior section through the middle segment of *gpa-3QL* reveals ten channel cilia embedded in the sheath cell. Some cilia have reduced diameters. Scale bar: 200 nm.

The cilia of the ADF, ASH, ASI, ASK and ADL neurons of adult *gpa-3QL* animals were shorter than those of wild-type adult animals (Fig. 2). Similar effects on ASI cilium length were observed with the transcriptional and the translational *gpa-4::GFP* fusions, which both visualize the complete cilium starting at the transition zone, and with the $p_{gpa\text{-}4}$*::tbb-4::mCherry* construct, which visualizes only the axoneme (Fig. 2; Table 1 and results not shown). The effect on cilium length was not fully penetrant; 14-82% of *gpa-*

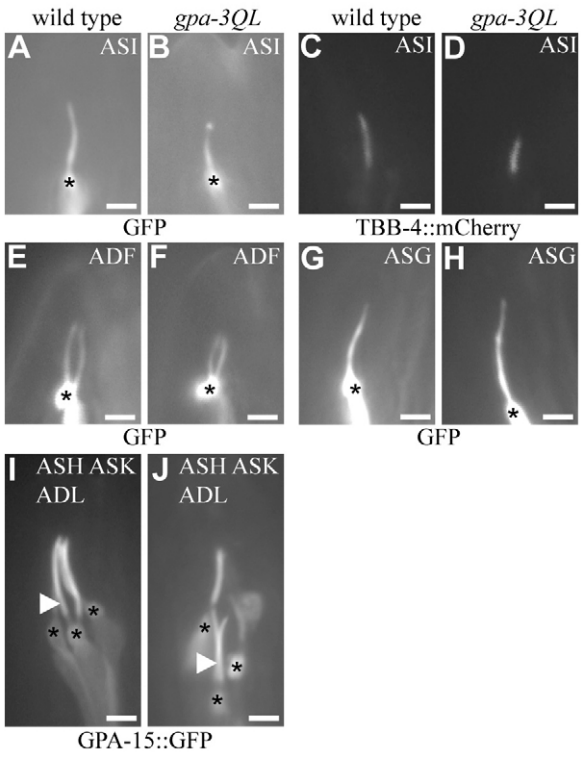

Fig. 2. *gpa-3QL* affects cilia length. (**A**,**B**) Visualization of ASI cilia using $p_{gpa\text{-}4}$*::gfp* in (A) wild-type and (B) *gpa-3QL(syIs25)* animals. (**C**,**D**) Visualization of ASI cilia using $p_{gpa\text{-}4}$*::tbb-4::mCherry* in (C) wild-type and (D) *gpa-3QL(syIs25)* animals. (**E**,**F**) Visualization of ADF cilia using $p_{srh\text{-}142}$*::gfp* in (E) wild-type and (F) *gpa-3QL(syIs25)* animals. (**G**,**H**) Visualization of ASG cilia using $p_{ops\text{-}1}$*::gfp* in (G) wild-type and (H) *gpa-3QL(syIs24)* animals. (**I**,**J**) Visualization of ASH, ASK and ADL cilia using $p_{gpa\text{-}15}$*::gpa-15::gfp* in (I) wild-type and (J) *gpa-3QL(syIs25)* animals. ADL cilia are indicated with an arrowhead. Asterisks indicate transition zones. Cilium length was determined in adult animals. Scale bars: 2 µm.

3QL animals had shorter cilia (Table 1). By contrast, the cilia of the ASG neurons were longer, and the ASE cilia of *gpa-3QL* animals did not differ significantly from those of wild type (Fig. 2; Table 1). Visualization of the ASH, ASK and ADL neurons using *gpa-15::gfp* showed that the middle segments and transition zones of their cilia were more spread out than in wild-type animals. In addition, the transition zones of the ASG and ADL cilia were displaced posteriorly (Fig. 2). There seems to be no general correlation between posterior displacement and cilium length, since ADL cilia were on average shorter, whereas ASG cilia were longer. Also loss-of-function of *gpa-3* affected cilium length, but to a lesser extent than *gpa-3QL*: ASI cilia were slightly longer and ASH, ASK and ADL cilia slightly shorter (Table 1).

The two *gpa-3QL* strains had different length cilia: The ASI cilia were only shorter in the *gpa-3QL(syIs25)* animals, whereas ASH, ASK and ADL cilia were shortened in both strains (Table 1). These differences might be caused by lower *gpa-3QL* expression in *gpa-3QL(syIs24)* animals, however immunohistochemistry and western blot analysis using anti-GPA-3 antibodies revealed similar, approximately 60-fold overexpression in the two *gpa-3QL* strains (supplementary material Fig. S2). However, this analysis did not address possible cell-specific variations in expression levels. To determine if the phenotypic differences were caused by variations

Table 1. *gpa-3QL* affects cilia length

Strain	Construct	ASI cells				ASH, ASK, ADL cells			ADF cells		ASG cells		ASE cells	
		gpa-4::gfp			*gpa-4::tbb-4::mCherry*	*gpa-15::gfp*			*srh-142::gfp*		*ops-1::gfp*		*flp-6::gfp*	
		Length	*n*	%	Length	*n*	Length	*n*	%	Length	*n*	Length	*n*	Length	*n*
Wild type		4.76±0.50	99	6	4.0±0.63	25	6.49±0.69	118	3	4.73±0.41	26	5.39±0.79	55	4.69±0.57	26
kap-1(ok676)		4.64±0.47	64	9			6.56±0.62	32	0			5.61±0.86	42		
osm-3(p802)		3.68±0.25[a]	74	89			4.53±0.34[a]	81	98			4.42±0.45[a]	37		
gpa-3(pk35)		5.15±0.57[b]	39	0			5.99±0.42[b]	49	4	4.86±0.59	42	5.47±0.94	75	4.91±0.66	34
kap-1; gpa-3		4.41±0.37[c]	44	14			6.03±0.76	52	13			4.98±0.69	57		
osm-3; gpa-3		3.69±0.20[a,c]	44	93			4.72±0.29[a,c]	42	91			4.71±0.55[b,c]	54		
gpa-3QL (syIs24)		4.75±0.66	36	14			4.89±0.67[a]	43	65	4.15±0.61[a]	28	6.74±1.31[a]	65	5.17±1.23	32
kap-1; gpa-3QL (syIs24)		4.43±0.54	42	21			5.63±0.59[a,c]	50	20			5.39±1.0[c]	67		
gpa-3QL (syIs25)		3.60±0.53[a]	38	82	2.83±0.50[a]	20	5.33±1.09[a]	57	56	3.66±0.42[a]	57	5.89±0.83	72	4.55±0.94	22
kap-1; gpa-3QL (syIs25)		4.12±0.46[a,c,d]	46	37			5.35±0.70[a]	61	38			5.62±1.11	17		
osm-3; gpa-3QL (syIs25)		3.10±0.32[a,e]	29	100			4.46±0.59[a,c]	48	85			4.32±0.62[a,c]	49		
gpa-4::gpa-3QL		4.42±0.57[a]	72	25			6.99±0.77[a]	63	2						

Data are the average lengths of cilia visualized with various GFP or mCherry fusion constructs ± the standard deviation (in µm); the number of measurements (*n*) and the percentage of short cilia (%). Significant differences in length are indicated; compared with wild-type animals ([a]$P<0.001$; [b]$P<0.005$); to the corresponding *gpa-3* allele ([c]$P<0.001$); to *kap-1* ([d]$P<0.001$) or to *osm-3* ([e]$P<0.001$). Cilium length was determined in adult animals.

in the expression of *gpa-3QL*, we injected the *gpa-3QL* construct at a range of concentrations into animals expressing the p_{gpa-4}*::gfp* transcriptional fusion or the p_{gpa-15}*::gpa-15::gfp* translational fusion and checked cilia length, morphology and posterior displacement of the basal bodies. The number and the severity of the ciliary defects correlated with the concentration of *gpa-3QL* injected (supplementary material Tables S1-S3), indicating that the variation in phenotypes is caused by differences in *gpa-3QL* expression levels.

Next, we examined whether activation of GPA-3 is important for its effect on cilium length. Overexpression of the wild-type *gpa-3* gene had a weaker effect on dye filling (maximally 37% Dyf at 170 ng/µl, compared with 85% for 170 ng/µl *gpa-3QL*), did not significantly shorten cilia length (P>0.01), and only mildly increased the percentage of animals with short cilia (supplementary material Table S4). These results suggest that overexpression of wild-type *gpa-3* affects cilia, but that activation of GPA-3 strongly enhances its effects.

The effect of *gpa-3QL* is inducible, reversible and cell-autonomous

To determine whether *gpa-3QL* acts specifically during ciliogenesis, which occurs at the embryonic threefold stage (Fujiwara et al., 1999), we generated animals that carried a heat-shock inducible *gpa-3QL* construct. Since both *gpa-3QL(syIs24)* and *syIs25* are dye-filling defective (Dyf), we first tested whether induction of *gpa-3QL* expression resulted in a dye-filling defect. Heat shock of mixed populations of animals resulted in dye filling defects in L1-L4 larvae and adult animals. We tested three independent strains, resulting in 91% (*gjEx1457*), 45% (*gjEx1456*) and 17% (*gjEx1292*) Dyf in adult animals (Fig. 3). The variation in Dyf phenotypes is probably caused by somatic mosaicism and variation in *gpa-3QL* expression between the strains. The induced Dyf phenotype was reversible since dye filling was restored 24 hours after heat-shock treatment (*gjEx1457* 6%, *gjEx1456* 1% and *gjEx1292* 2% Dyf; Fig. 3). Also cilium length of *gjEx1457* animals was reduced 2 hours after heat shock, but recovered to normal length within 24 hours (average length before heat shock 4.91±0.31 µm (n=18; 0% short cilia), 2 hours after heat shock 4.32±0.63 µm (n=36, P<0.005 compared with before or 24 hours after heat shock; 42% short cilia) and 24 hours after heat shock 4.85±0.44 µm (n=30, 0% short cilia). These results indicate that the effect of *gpa-3QL* is not restricted to a specific developmental time-window, but affects a regulatory mechanism important for cilia structure throughout the life of *C. elegans*.

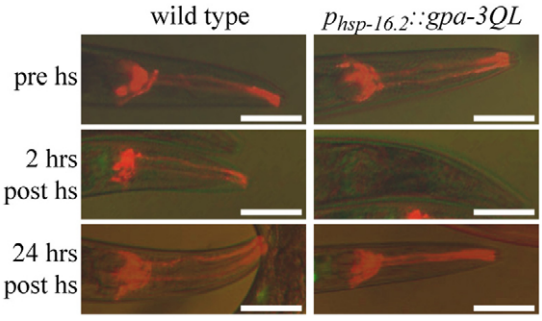

Fig. 3. The effect of *gpa-3QL* on cilia is inducible and reversible. DiI dye filling of animals expressing *gpa-3QL* under control of the *hsp-16.2* heat-shock promoter and wild-type controls before treatment, 2 hours after heat shock (hs), and 24 hours after heat shock. Scale bars: 50 µm.

gpa-3 is only expressed in ten pairs of amphid sensory neurons, in the PHA and PHB phasmid neurons and in the AIZ and PVT interneurons (Lans et al., 2004; Zwaal et al., 1997). To determine whether the effect of *gpa-3QL* on cilia length is cell autonomous, or whether expression in one pair of sensory neurons also affects cilia morphology of other neurons, we generated animals that express *gpa-3QL* specifically in the ASI neurons, using a p_{gpa-4}*::gpa-3QL* construct. We observed significantly shorter ASI cilia in animals expressing p_{gpa-4}*::gpa-3QL*. However, we did not observe shortening of cilia of the neighboring neuron ADL, ASK or ASH in two independent transgenic strains (Table 1). These results suggest that the effect of *gpa-3QL* on cilia length is cell-autonomous, although we cannot exclude the possibility that expression is too low to affect ASH, ASK and ADL cilia length.

Mutation of *gpa-3* affects the coordination of kinesin-II and OSM-3

Cilium length is thought to be regulated by modulation of transport in the cilium (Dentler, 2005; Engel et al., 2009; Marshall et al., 2005; Pan and Snell, 2005). Hence we set out to see if mutation of *gpa-3* affects IFT. First, we determined whether the effects of mutation of *gpa-3* on cilia length require either of the two kinesin-2 motors. *kap-1; gpa-3QL(syIs25)* double mutants had significantly longer ASI cilia than *gpa-3QL(syIs25)* animals and *kap-1; gpa-3QL(syIs24)* double mutants had longer ADL, ASH and ASK cilia and shorter ASG cilia than *gpa-3QL(syIs24)* animals (Table 1). *osm-3; gpa-3QL(syIs25)* animals had even shorter ASI cilia than *osm-3* animals. Also the effect of *gpa-3(lf)* on the length of ASI cilia was suppressed in *kap-1; gpa-3* animals. These results suggest that the effect of *gpa-3* mutation on cilia length is partially mediated by kinesin-II and might also be mediated by OSM-3.

Second, we determined the localization of KAP-1::GFP and OSM-3::GFP to visualize the two kinesin-2 motors, the dynein light intermediate chain XBX-1::GFP, the complex A protein CHE-11::GFP (IFT140 in human) and the complex B protein OSM-1::GFP (IFT172 in human) (Qin et al., 2001; Schafer et al., 2003; Signor et al., 1999; Snow et al., 2004). All these proteins could be detected at their normal localization in *gpa-3QL* animals (results not shown). It must be noted that ciliary defects of *gpa-3QL* animals were difficult to visualize using these constructs, probably because they are expressed in all amphid channel cilia and because of the variability of the defects.

Third, we measured transport rates of IFT components (Fig. 4; supplementary material Table S5; representative examples of kymographs are presented in supplementary material Fig. S3). In the middle segments of wild-type animals, kinesin-II and OSM-3 both traveled at 0.7 µm/second. In the absence of kinesin-II, OSM-3 moved faster (1.17 µm/second) and in the absence of OSM-3, kinesin-II moved slower (0.49 µm/second). In the distal segments, OSM-3 moved at 1.07 µm/second. These speeds are in agreement with previous reports (Ou et al., 2005; Snow et al., 2004). We found that in the middle segments of both *gpa-3QL* and *gpa-3(lf)* animals OSM-3::GFP-containing particles moved at approximately 1 µm/second. KAP-1::GFP speeds were not as strongly affected, resulting in speeds of approximately 0.60 µm/second. In double mutants between *gpa-3QL* or *gpa-3(lf)* and *kap-1* or *osm-3* the kinesins moved at approximately the same speeds as in *kap-1* or *osm-3* single mutants, suggesting that mutation of *gpa-3* does not affect the velocity of the kinesins per se, but rather that the two

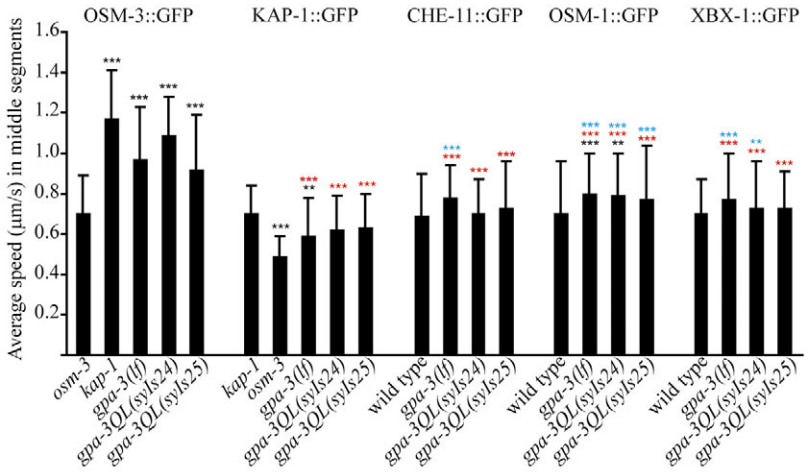

Fig. 4. Mutation of *gpa-3* affects transport speeds. Average speeds ± the standard deviation of OSM-3::GFP, KAP-1::GFP, CHE-11::GFP, OSM-1::GFP and XBX-1::GFP in various genetic backgrounds. Statistically significant differences compared with speeds in wild type are indicated in black, compared with OSM-3::GFP speeds in the same genetic background in red, and compared with KAP-1::GFP in the same genetic background in blue (***P<0.001, **P<0.005). Speeds were determined in adult animals. Further details can be found in supplementary material Table S5.

kinesin motors do not travel together in the same IFT particles. We observed no effects on the speeds in the distal segments (supplementary material Table S5).

Separation of OSM-3 and kinesin-II can be due to (1) a separation of the complex A and B proteins, as described for *bbs-7* and *bbs-8* animals (Ou et al., 2005), (2) a failure of one of the motors to link to the complex A or B scaffold, as described for *dyf-5* or *dyf-1* animals (Burghoorn et al., 2007; Ou et al., 2005), or (3) by an unknown mechanism. To discriminate between these possibilities we measured the anterograde speeds of fluorescently tagged complex A protein CHE-11/IFT140, complex B protein OSM-1/IFT172 and dynein subunit XBX-1 (Fig. 4; supplementary material Table S5). The velocities in the middle segments of wild-type animals were all 0.7 μm/second. In *gpa-3QL* and in *gpa-3(lf)* animals these three proteins traveled only slightly faster than 0.7 μm/second, at a rate intermediate to that of the two kinesins, suggesting that these proteins move together. These findings do not fit either of the two mechanisms described before (Burghoorn et al., 2007; Ou et al., 2005) and suggest a novel mechanism that regulates the coordination of IFT.

Exposure to dauer pheromone affects the coordination of the two kinesins

gpa-3 plays a role in dauer development: *gpa-3QL* animals show a dauer constitutive phenotype, whereas *gpa-3(lf)* animals are dauer defective (Zwaal et al., 1997). Interestingly, dauer development involves alterations in the position and structure of several cilia, including a posterior displacement of the cilia of the ASI and ASG neurons (Albert and Riddle, 1983). Peckol et al. (Peckol et al., 2001) have shown that five of the six pairs of cells that normally take up fluorescent dye do so, with the exception of ASI. Measurement of ASI cilia length using GPA-4::GFP showed that exposure to dauer pheromone did not result in shorter cilia (results not shown), confirming that the ASI dye-filling defect does not result from cilia shortening, but may be the result of posterior displacement or by another structural change of the cilia (Albert and Riddle, 1983; Peckol et al., 2001).

To determine whether dauer pheromone exposure affects IFT protein motility, we measured transport rates of KAP-1::GFP, OSM-3::GFP, OSM-1::GFP and CHE-11::GFP in L2 and L2d animals. In the middle segments of untreated wild-type L2 larvae KAP-1::GFP and OSM-3::GFP traveled at a speed of approximately 0.7 μm/second, which is comparable with the speeds in young adult animals. Exposure of larvae to dauer pheromone decreased KAP-1::GFP speed to 0.56 μm/second and increased OSM-3::GFP speed to 0.89 μm/second, whereas complex A and B proteins moved at approximately 0.7 μm/second (Fig. 5; supplementary material Table S6). Thus, exposure to dauer pheromone uncouples kinesin-II and OSM-3 kinesin, very similar to gain- or loss-of-function of *gpa-3*.

To determine whether the effect of dauer pheromone on the speeds of the kinesins is mediated by GPA-3, we measured KAP-

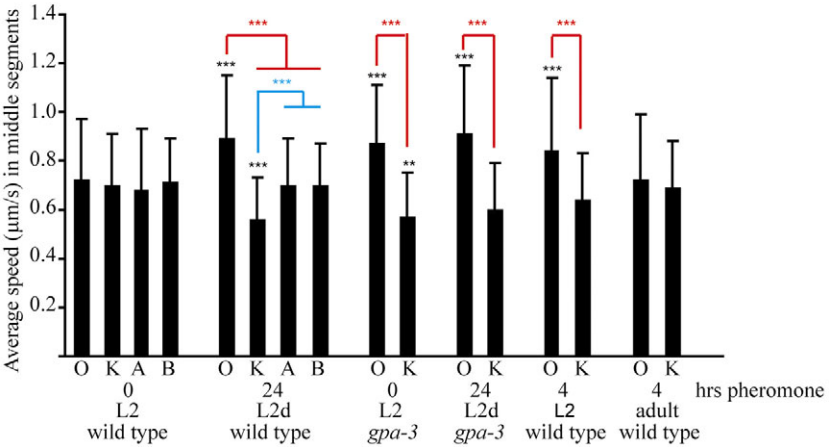

Fig. 5. Exposure to dauer pheromone affects transport speeds. Average speeds ± the standard deviation of OSM-3::GFP (O), KAP-1::GFP (K), CHE-11::GFP (A) and OSM-1::GFP (B) in L2, L2d or adult wild-type or *gpa-3(lf)* animals after 0, 4, or 24 hours exposure to dauer pheromone. Statistically significant differences compared with speeds in wild type L2 animals are indicated in black, compared with OSM-3::GFP under the same experimental conditions in red, and compared with KAP-1::GFP under the same experimental conditions in blue (***P<0.001, **P<0.005). Further details can be found in supplementary material Table S6.

1::GFP and OSM-3::GFP transport rates in *gpa-3(lf)* L2 and L2d animals. Exposure to dauer pheromone did not affect the speeds of the two kinesins in the middle segments of *gpa-3(lf)* larvae: KAP-1::GFP traveled at a speed of approximately 0.6 μm/second, whereas OSM-3::GFP moved at approximately 0.9 μm/second (Fig. 5; supplementary material Table S6). Since exposure to dauer pheromone and *gpa-3(lf)* have very similar effects on the kinesin speeds, and these effects are not cumulative, this suggests that *gpa-3* functions in the same pathway as exposure to dauer pheromone.

To test if exposure to dauer pheromone has an acute effect on IFT, we exposed L1 larvae for 4 hours to dauer-inducing concentrations of dauer pheromone, and measured speeds of KAP-1::GFP and OSM-3::GFP. In these animals, short exposure to dauer pheromone had a similar effect on OSM-3::GFP speeds as 24-28 hours exposure, but had no significant effect on KAP-1::GFP speeds (Fig. 5; supplementary material Table S6). These results indicate that dauer pheromone has an acute effect on the regulation of IFT in larvae.

Finally, we exposed adult animals to dauer pheromone for 4 hours, and measured IFT speeds. However, there were no effects on kinesin speeds in these animals (Fig. 5; supplementary material Table S6), suggesting that there is a specific developmental time window in which dauer pheromone can modulate IFT.

Discussion

We show that in *gpa-3QL* and *gpa-3(lf)* animals and in larvae exposed to dauer pheromone IFT is perturbed: kinesin-II speed is reduced and OSM-3 kinesin speed is increased, indicating that they move separately. The velocities of KAP-1::GFP and OSM-3::GFP in these animals suggest that this separation is not absolute. Based on the average speeds of the two motors we calculated that in the cilia of *gpa-3(lf)* animals approximately 55% of the motors move separately, in *gpa-3QL(syIs24)* approximately 60% and in *gpa-3QL(syIs25)* approximately 40%, leaving a significant background of non-separated complexes. Surprisingly, complex A and B proteins travel at rates that are not or only slightly different from those in wild-type animals, and that are intermediate to the rates of the kinesins in *gpa-3* or pheromone-exposed animals. This particular combination of speeds for IFT components does not fit a separation as found in *bbs-7* and *bbs-8* mutants, where kinesin-II travels together with the complex A proteins and OSM-3 travels with the complex B proteins (Ou et al., 2005), or a docking defect as found in *dyf-5* or *dyf-1* animals (Burghoorn et al., 2007; Ou et al., 2005).

We propose two possible explanations for these IFT speeds. First, mutation of *gpa-3* or exposure of larvae to dauer pheromone could alter the stoichiometry of kinesin motors on the IFT particles. Depending on its penetrance, this would change the molar ratio of motors on the IFT particles, which would affect their transport rates (Pan et al., 2006), or even result in a full separation, where IFT particles are loaded exclusively with kinesins-II or OSM-3. In both cases, the velocities of complex A and B proteins would be approximately the mean of the speeds of kinesin-II and OSM-3, because these proteins are transported by both kinesins (supplementary material Fig. S4A). The second possibility is that in *gpa-3* mutant animals and in dauer pheromone-treated larvae the ability of the kinesins to dock onto the IFT particles is affected, resulting in pools of free kinesins. IFT particles, containing complex A and B proteins, are then only transported by kinesin-II and OSM-3 together, at approximately 0.7 μm/seconds, while non-associated kinesin-II and OSM-3 travel at 0.5 and 1.2 μm/seconds, respectively (supplementary material Fig. S4B).

The first scenario suggests the presence of discernable subgroups of kinesin-II- or OSM-3-transported particles. However, plotting the speeds of OSM-1::GFP, CHE-11::GFP and XBX-1::GFP in the middle segments of *gpa-3QL* cilia did not reveal a clear bimodal distribution (supplementary material Fig. S5). It must be noted that a bimodal distribution might be masked by the large variance in the speeds of the particles, and by the sizable fraction of particles transported by both motor complexes. However, data presented by Imanishi et al. (Imanishi et al., 2006) suggest that OSM-3 exists in an autoinhibited state, which is thought to be relieved by binding to IFT particles. This finding would argue against movement of free OSM-3 and thus possibly against our second model. Further analysis is required to resolve this issue.

The IFT machinery not only consists of motor proteins and adapter proteins, but also contains regulatory proteins, such as the Rab-like G proteins IFT27 and Rab8 (Nachury et al., 2007; Qin et al., 2007). This raises the question of whether GPA-3 is also part of the IFT machinery. Although GPA-3QL and GPA-3 localize to the cilia, GPA-3::GFP does not localize to IFT particles, nor could we measure motility of GPA-3::GFP in the cilia. We therefore favor the possibility that GPA-3 acts at the membrane to relay GPCR activation into intracellular signaling, which acts on the coordination of kinesin motors in the cilia.

Our finding that exposure to dauer pheromone affects the speeds of kinesin-II and OSM-3 in a very similar way as mutation of *gpa-3* and that these effects are not cumulative, suggests that *gpa-3* functions in the same pathway as dauer pheromone to regulate the coordination of IFT kinesins. Zwaal et al. (Zwaal et al., 1997) previously found that *gpa-3* probably functions upstream in the DAF-7/TGFβ pathway to regulate dauer formation. It is unclear if the regulation of IFT depends on the DAF-7/TGFβ pathway or functions upstream or in parallel of this pathway. Preliminary data suggest that exposure to dauer pheromone and activation of GPA-3 on the one hand induces the dauer pathway via inactivation of DAF-11 and DAF-7, and on the other hand affects the coordination of IFT by the two kinesins. Further experiments are required to resolve this issue.

It is puzzling that exposure to dauer pheromone, dominant active mutation of *gpa-3* and loss-of-function of *gpa-3* have similar effects on IFT, i.e. they partially uncouple the two kinesins, whereas dauer pheromone and *gpa-3QL* induce dauer formation and affect cilia morphology, and *gpa-3(lf)* suppresses dauer formation and does not affect cilia morphology. At present, we have no data that explain these findings. However, it might be that although activation and inactivation of *gpa-3* have similar effects on the coupling of the two kinesins, they might have differential effects on cargo loading. Pan and Snell have shown that shortening of the cilia in *Chlamydomonas* is the result of increased IFT shuttling and reduced anterograde cargo loading (Pan and Snell, 2005). An intriguing possibility is that in *gpa-3QL* animals the subset of IFT particles transported only by OSM-3 does not contain cargo, whereas the kinesin-II-transported particles contain molecules that maintain the integrity of the cilia, resulting in shortening of the distal segments, but leaving the middle segments intact. In *gpa-3(lf)* animals, the loading of kinesins could be the other way around, thus leaving the cilia intact. To test this model one would have to be able to differentiate the subsets of IFT particles, for example by their cargo. Such analyses would also help to choose between the two possible IFT models. Thus far, we have not identified such cargo molecules.

Recently, Engel et al. (Engel et al., 2009) found an inverse correlation between IFT particle size and the length of

Chlamydomonas flagella: shorter flagella contained larger IFT particles or trains. This finding suggests that cilia and flagella length might be regulated by modulating IFT particle size. Unfortunately, we were not able to analyze IFT particle size in our kymographs, because of the background fluorescence caused by expression of the GFP fusion constructs in other cilia and because of the incomplete penetrance of *gpa-3QL*.

What would be the physiological significance of uncoupling of kinesin-II and OSM-3 kinesin by dauer pheromone and G protein signaling? First of all, exposure to dauer pheromone affects cilia structure, since it affects ASI dye filling and results in posterior displacement of the ASI and ASG cilia (Albert and Riddle, 1983), although it does not result in shortening of the cilia. Over activation of this pathway, in *gpa-3QL* animals, strongly affects the morphology of the amphid channel cilia: many cilia are shorter, some are longer, and some are displaced posteriorly. Although no obvious changes in cilia structure have been observed in *gpa-3(lf)* animals, it is possible that loss-of-function of *gpa-3* has an opposite effect, resulting in stabilization of the cilia. In addition to regulating cilia morphology, we expect that coordinated coupling of kinesin-II and OSM-3 also allows relocalization of receptors or other signaling molecules in the cilia. For example, signaling molecules that are normally transported to the distal end by OSM-3 can be cleared from the distal segment by excluding them from OSM-3-transported particles. These effects may serve to alter the sensitivity of the animal to certain environmental cues and for example reinforce the choice to become a dauer.

Many components of the IFT machinery and the signaling pathways are remarkably well conserved in evolution. This suggests that similar mechanisms in which external cues can influence cilia structure also exist in other organisms. A recent report by Besschetnova et al. (Besschetnova et al., 2010) and our results illustrate this concept in organisms as diverse as mammals and worms.

Materials and Methods

Strains and constructs

The alleles used were Bristol N2 (wild type), *gpa-3(pk35)IV*, *gpa-3QL(syIs25)X*, *gpa-3QL(syIs24)IV*, *kap-1(ok676)II* and *osm-3(p802)IV*. GFP reporters used were p_{gpa-4}*::gfp*, p_{gpa-15}*::gfp*, $p_{srh-142}$*::gfp*, p_{ops-1}*::gfp*, p_{flp-6}*::gfp*, *che-11::gfp*, *osm-1::gfp*, *osm-3::gfp*, *kap-1::gfp* and *xbx-1::gfp* (Jansen et al., 1999; Li et al., 1999; Orozco et al., 1999; Qin et al., 2001; Sagasti et al., 1999; Sarafi-Reinach and Sengupta, 2000; Schafer et al., 2003; Signor et al., 1999). All GFP reporters were crossed into the different mutant backgrounds, except when indicated. A heat-shock-inducible *gpa-3QL* construct ($p_{hsp-16.2}$*::gpa-3QL*) was generated by subcloning *gpa-3QL* into the pPD49.78 vector (Mello and Fire, 1995). A p_{gpa-4}*::tbb-4::mCherry* construct was made by fusing *tbb-4::gfp* (a gift from Maureen Barr, Rutgers University, Newark, NJ) to the translation start of *gpa-4*, in p_{gpa-4}*::gfp*, and exchanging *gfp* for *mCherry* (a gift from Roger Tsien, University of California, San Diego, CA). A p_{gpa-4}*::gpa-3QL* construct was made by fusing the *gpa-4* promoter to the translation start of *gpa-3QL* in pJMG3QL (Zwaal et al., 1997). Microinjections were performed as described previously (Mello and Fire, 1995).

Immunoblotting

Total lysates of 80 worms were solubilized with SDS-PAGE sample buffer. After electrophoresis on a 15% SDS-PAGE gel, proteins were transferred to membranes and probed with antibodies against GPA-3 [clone AYW9, affinity purified (Lans et al., 2004), secondary antibody Amersham DαRab HRP, detected with ECL, Amersham] and against α-tubulin (Invitrogen clone B512, secondary antibody Li-COR DαMouse Infrared 795, detected with an Odyssey infrared imager). GPA-3 protein levels were estimated by averaging GPA-3 band intensities (normalized against α-tubulin) of three different exposures of four blots each. An example illustrating GPA-3QL overexpression is given in supplementary material Fig. S2.

Microscopy

The location of fluorescent proteins and cilia was examined using a Zeiss LSM 510 confocal microscope. Cilia lengths were measured using a Zeiss Imager Z1 microscope, by measuring the length from the transition zone to the distal tip of the cilium. In all cases cilium length was determined in adult animals. The percentage of short cilia, which were considered to be smaller than the intersection between the distribution plots of wild-type and *osm-3* cilia lengths (4.04 µm for GPA-4::GFP and 5.18 µm for GPA-15::GFP), was determined. Dye filling was performed using 0.1 mg/ml DiI (Molecular Probes) as described previously (Perkins et al., 1986). Immunofluorescence using polyclonal rabbit antibody against GPA-3 was performed as described previously (Lans et al., 2004). For EM, animals were fixed in 3% glutaraldehyde for 16 hours, followed by post-fixation in 1% osmium tetroxide for 2 hours. Subsequently, animals were orientated in special moulds and embedded in Epon according to standard procedures. Ultrathin sections were cut with a Reichert ultramicrotome, stained with uranyl acetate and lead nitrate and examined with a Philips CM100 electron microscope at 80 kV.

Heat shock

Mixed populations of well-fed animals were heat-shocked at 30°C for 15 hours, allowed to recover at room temperature for 2 hours and subsequently analyzed using dye filling or by measuring cilium length as described above.

Live imaging of IFT particles

Live imaging of the GFP-tagged IFT particles was carried out as described previously (Orozco et al., 1999; Snow et al., 2004). Images were acquired on a Zeiss LSM 510 confocal microscope with a 63× (NA 1.4) objective. Worms were mounted on an agarose pad and anaesthetized with 10 mM levamisole. Kymographs were generated in ImageJ with the kymograph plugin, written by J. Rietdorf.

Dauer analysis

Dauer pheromone was isolated as described previously (Golden and Riddle, 1982). Adult animals were allowed to lay eggs for 3 hours on plates containing dauer pheromone, at a concentration resulting in approx. 90% dauers in wild-type animals. Larvae were analyzed after 24-28 hours (L2 or L2d larvae) or after 52-58 hours (L4 or dauer animals) at 25°C.

Statistics and calculations

Statistical significance was determined using an ANOVA, followed by a Bonferroni post-hoc test.

The observed *osm-3::gfp* and *kap-1::gfp* speeds are each composed of the speed of the fraction that moves together with the other kinesin (at 0.70 µm/seconds, *osm-3::gfp* speed in *osm-3* animals, or *kap-1::gfp* speed in *kap-1* animals) and the fraction that moves separately (at 1.17 µm/seconds, *osm-3::gfp* speed in *kap-1* animals, or 0.49 µm/seconds, *kap-1::gfp* speed in *osm-3* animals). The formula used to calculate the fraction of *osm-3* that moves separately (x) is: $x_{osm-3}=(v_{gpa-3}-v_{together})/(v_{max}-v_{together})$, where v_{gpa-3} is the *osm-3::gfp* speed measured in a *gpa-3* mutant, $v_{together}$ is the *osm-3::gfp* speed measured in *osm-3* animals and v_{max} is the *osm-3::gfp* speed measured in *kap-1* animals. The formula used to calculate the fraction of *kap-1* that moves separately (x) is: $x_{kap-1}=(v_{gpa-3}-v_{together})/(v_{max}-v_{together})$, where v_{gpa-3} is the *kap-1::gfp* speed measured in a *gpa-3* mutant, $v_{together}$ is the *kap-1::gfp* speed measured in *kap-1* animals and v_{max} is the *kap-1::gfp* speed measured in *osm-3* animals.

We thank E. Severijnen, R. Koppenol and E. Efimenko for technical assistance, the *Caenorhabditis* Genetics Center, J. Mendel, P. Sternberg, M. Barr, A. Fire, C. Haycraft, B. Yoder, G. Ou, J. Scholey, C. Li, P. Sengupta and R. Tsien for *C. elegans* strains and constructs. This work was supported by the Centre for Biomedical Genetics and a PKD Foundation Grant to G.J.

Supplementary material available online at
http://jcs.biologists.org/cgi/content/full/123/??/????/DC1

References

Albert, P. S. and Riddle, D. L. (1983). Developmental alterations in sensory neuroanatomy of the *Caenorhabditis elegans* dauer larva. *J. Comp. Neurol.* **219**, 461-481.

Bae, Y.-K., Qin, H., Knobel, K. M., Hu, J., Rosenbaum, J. L. and Barr, M. M. (2006) General and cell-type specific mechanisms target TRPP2/PKD-2 to cilia. *Development* **133**, 3859-3870.

Bengs, F., Scholz, A., Kuhn, D. and Wiese, M. (2005). LmxMPK9, a mitogen-activated protein kinase homologue affects flagellar length in *Leishmania mexicana*. *Mol. Microbiol.* **55**, 1606-1615.

Berman, S. A., Wilson, N. F., Haas, N. A. and Lefebvre, P. A. (2003). A novel MAP kinase regulates flagellar length in *Chlamydomonas*. *Curr. Biol.* **13**, 1145-1149.

Besschetnova, T. Y., Kolpakova-Hart, E., Guan, Y., Zhou, J., Olsen, B. R. and Shah, J. V. (2010). Identification of signaling pathways regulating primary cilium length and flow-mediated adaptation. *Curr. Biol.* **20**, 182-187.

Blaineau, C., Tessier, M., Dubessay, P., Tasse, L., Crobu, L., Pagès, M. and Bastien, P. (2007). A novel microtubule-depolymerizing kinesin involved in length control of a eukaryotic flagellum. *Curr. Biol.* **17**, 778-782.

Burghoorn, J., Dekkers, M. P. J., Rademakers, S., de Jong, T., Willemsen, R. and Jansen, G. (2007). Mutation of the MAP kinase DYF-5 affects docking and undocking

of kinesin-2 motors and reduces their speed in the cilia of *Caenorhabditis elegans*. *Proc. Natl. Acad. Sci. USA* **104**, 7157-7162.

Cuppen, E., van der Linden, A. M., Jansen, G. and Plasterk, R. H. A. (2003). Proteins interacting with *Caenorhabditis elegans* Gα subunits. *Comp. Funct. Genom.* **4**, 479-491.

Dentler, W. (2005). Intraflagellar transport (IFT) during assembly and disassembly of *Chlamydomonas* flagella. *J. Cell Biol.* **170**, 649-659.

Engel, B. D., Ludington, W. B. and Marshall, W. F. (2009). Intraflagellar transport particle size scales inversely with flagellar length: revisiting the balance-point length control model. *J. Cell Biol.* **187**, 81-89.

Evans, J. E., Snow, J. J., Gunnarson, A. L., Ou, G., Stahlberg, H., McDonald, K. L. and Scholey, J. M. (2006). Functional modulation of IFT kinesins extends the sensory repertoire of ciliated neurons in *Caenorhabditis elegans*. *J. Cell Biol.* **172**, 663-669.

Fujiwara, M., Ishihara, T. and Katsura, I. (1999). A novel WD40 protein, CHE-2, acts cell-autonomously in the formation of *C. elegans* sensory cilia. *Development* **126**, 4839-4848.

Golden, J. W. and Riddle, D. L. (1982). A pheromone influences larval development in the nematode *Caenorhabditis elegans*. *Science* **218**, 578-580.

Imanishi, M., Endres, N. F., Gennerich, A. and Vale, R. D. (2006). Autoinhibition regulates the motility of the *C. elegans* intraflagellar motor OSM-3. *J. Cell Biol.* **174**, 931-937.

Jansen, G., Thijssen, K. L., Werner, P., van derHorst, M., Hazendonk, E. and Plasterk, R. H. A. (1999). The complete family of genes encoding G proteins of *Caenorhabditis elegans*. *Nat. Genet.* **21**, 414-419.

Lans, H., Rademakers, S. and Jansen, G. (2004). A network of stimulatory and inhibitory Gα-subunits regulates olfaction in *Caenorhabditis elegans*. *Genetics* **167**, 1677-1687.

Li, C., Kim, K. and Nelson, L. S. (1999). FMRFamide-related neuropeptide gene family in *Caenorhabditis elegans*. *Brain Res.* **848**, 26-34.

Marshall, W. F., Qin, H., Brenni, M. R. and Rosenbaum, J. L. (2005). Flagellar length control system: testing a simple model based on intraflagellar transport and turnover. *Mol. Biol. Cell* **16**, 270-278.

Mello, C. and Fire, A. (1995). DNA transformation. In *Caenorhabditis elegans: Modern Biological Analysis of an Organism* (ed. H. F. Epstein and D. C. Shakes), pp. 451-482. San Diego: Academic Press.

Mukhopadhyay, S., Lu, Y., Shaham, S. and Sengupta, P. (2008). Sensory signaling-dependent remodeling of olfactory cilia architecture in *C. elegans*. *Dev. Cell* **14**, 762-774.

Nachury, M. V., Loktev, A. V., Zhang, Q., Westlake, C. J., Peränen, J., Merdes, A., Slusarski, D. C., Scheller, R. H., Bazan, J. F., Sheffield, V. C. et al. (2007). A core complex of BBS proteins cooperates with the GTPase Rab8 to promote ciliary membrane biogenesis. *Cell* **129**, 1201-1213.

Orozco, J. T., Wedaman, K. P., Signor, D., Brown, H., Rose, L. and Scholey, J. M. (1999). Movement of motor and cargo along cilia. *Nature* **398**, 674-674.

Ou, G. E., Blacque, O., Snow, J. J., Leroux, M. R. and Scholey, J. M. (2005). Functional coordination of intraflagellar transport motors. *Nature* **436**, 583-587.

Pan, J. and Snell, W. J. (2005). *Chlamydomonas* shortens its flagella by activating axonemal disassembly, stimulating IFT particle trafficking, and blocking anterograde cargo loading. *Dev. Cell* **9**, 431-438.

Pan, X., Ou, G., Civelekoglu-Scholey, G., Blacque, O. E., Endres, N. F., Tao, L., Mogilner, A., Leroux, M. R., Vale, R. D. and Scholey, J. M. (2006). Mechanism of transport of IFT particles in *C. elegans* cilia by the concerted action of kinesin-II and OSM-3 motors. *J. Cell Biol.* **174**, 1035-1045.

Peckol, E. L., Troemel, E. R. and Bargmann, C. I. (2001). Sensory experience and sensory activity regulate chemosensory receptor gene expression in *Caenorhabditis elegans*. *Proc. Natl. Acad. Sci. USA* **98**, 11032-11038.

Perkins, L. A., Hedgecock, E. M., Thomson, J. N. and Culotti, J. G. (1986). Mutant sensory cilia in the nematode *Caenorhabditis elegans*. *Dev. Biol.* **117**, 456-487.

Qin, H., Rosenbaum, J. L. and Barr, M. M. (2001). An autosomal recessive polycystic kidney disease gene homolog is involved in intraflagellar transport in *C. elegans* ciliated sensory neurons. *Curr. Biol.* **11**, 457-461.

Qin, H., Wang, Z., Diener, D. and Rosenbaum, J. (2007). Intraflagellar transport protein 27 is a small G protein involved in cell-cycle control. *Curr. Biol.* **17**, 193-202.

Quarmby, L. M. (2004). Cellular deflagellation. *Int. Rev. Cytol.* **233**, 47-91.

Riddle, D. L. and Albert, P. S. (1997). Genetic and environmental regulation of dauer larva development. In *C. elegans II* (ed. D. L. Riddle, T. Blumenthal, B. J. Meyer and J. R. Priess), pp. 739-768. New York: Cold Spring Harbor Laboratory Press.

Sagasti, A., Hobert, O., Troemel, E. R., Ruvkun, G. and Bargmann, C. I. (1999). Alternative olfactory neuron fates are specified by the LIM homeobox gene *lim-4*. *Genes Dev.* **13**, 1794-1806.

Sarafi-Reinach, T. R. and Sengupta, P. (2000). The forkhead domain gene *unc-130* generates chemosensory neuron diversity in *C. elegans*. *Genes Dev.* **14**, 2472-2485.

Schafer, J. C., Haycraft, C. J., Thomas, J. H., Yoder, B. K. and Swoboda, P. (2003). XBX-1 encodes a dynein light intermediate chain required for retrograde intraflagellar transport and cilia assembly in *Caenorhabditis elegans*. *Mol. Biol. Cell* **14**, 2057-2070.

Signor, D., Wedaman, K. P., Orozco, J. T., Dwyer, N. D., Bargmann, C. I., Rose, L. S. and Scholey, J. M. (1999). Role of a class DHC1b dynein in retrograde transport of IFT motors and IFT raft particles along cilia, but not dendrites, in chemosensory neurons of living *Caenorhabditis elegans*. *J. Cell Biol.* **147**, 519-530.

Snow, J. J., Ou, G., Gunnarson, A. L., Walker, M. R. S., Zhou, H. M., Brust-Mascher, I. and Scholey, J. M. (2004). Two anterograde intraflagellar transport motors cooperate to build sensory cilia on *C. elegans* neurons. *Nat. Cell Biol.* **6**, 1109-1113.

Sorokin, S. (1962). Centrioles and the formation of rudimentary cilia by fibroblasts and smooth muscle cells. *J. Cell Biol.* **15**, 363-377.

Tam, L.-W., Wilson, N. F. and Lefebvre, P. A. (2007). A CDK-related kinase regulates the length and assembly of flagella in *Chlamydomonas*. *J. Cell Biol.* **176**, 819-829.

Wang, Q., Pan, J. and Snell, W. J. (2006). Intraflagellar transport particles participate directly in cilium-generated signaling in *Chlamydomonas*. *Cell* **125**, 549-562.

Ward, S., Thomson, N., White, J. G. and Brenner, S. (1975). Electron microscopical reconstruction of the anterior sensory anatomy of the nematode *Caenorhabditis elegans*. *J. Comp. Neurol.* **160**, 313-337.

Zwaal, R. R., Mendel, J. E., Sternberg, P. W. and Plasterk, R. H. A. (1997). Two neuronal G proteins are involved in chemosensation of the *Caenorhabditis elegans* dauer-inducing pheromone. *Genetics* **145**, 715-727.